Bounce- and MLT-averaged diffusion coefficients in a physics-based magnetic field geometry obtained from RAM-SCB for the 17 March 2013 storm

Zhao, Lei
Yu, Yiqun
Delzanno, Gian Luca
Jordanova, Vania Koleva

Bounce- and MLT-averaged diffusion coefficients in a physics-based magnetic field geometry obtained from RAM-SCB for the March 17 2013 storm

Lei Zhao[1], Yiqun Yu[1], Gian Luca Delzanno[1], and Vania K. Jordanova[2]

———

Corresponding author: L. Zhao, Center for Nonlinear Studies (CNLS) and T-5 Applied Mathematics and Plasma Physics, Los Alamos National Laboratory, Los Alamos, USA. (lzhao@lanl.gov)

[1]Theoretical Division, Los Alamos

National Laboratory, Los Alamos, New

Mexico, USA

[2]Intelligence and Space Research Division,

Los Alamos National Laboratory, Los

Alamos, New Mexico, USA

Abstract.   Local acceleration via whistler wave and particle interaction

plays a significant role in particle dynamics in the radiation belt. In this work

we explore gyro-resonant wave-particle interaction and quasi-linear diffusion

in different magnetic field configurations related to the March 17 2013 storm.

We consider the Earth's magnetic dipole field as a reference, and compare

the results against non-dipole field configurations corresponding to quiet and

stormy conditions. The latter are obtained with RAM-SCB, a code that mod-

els the Earth's ring current and provides a realistic modeling of the Earth's

magnetic field. By applying quasi-linear theory, the bounce- and MLT-averaged

electron pitch angle, mixed term and energy diffusion coefficients are calcu-

lated for each magnetic field configuration. For radiation belt (~ 1 MeV) and

ring current (~ 100 keV) electrons, it is shown that at some MLTs the bounce-

averaged diffusion coefficients become rather insensitive to the details of the

magnetic field configuration, while at other MLTs storm conditions can ex-

pand the range of equatorial pitch angles where gyro-resonant diffusion oc-

curs and significantly enhance the diffusion rates. When MLT average is per-

formed at drift shell L = 4.25 (a good approximation to drift average),

the diffusion coefficients become quite independent of the magnetic field con-

figuration for relativistic electrons, while the opposite is true for lower en-

ergy electrons.

    These results suggest that, at least for the 17 March 2013 storm and for

$L \lesssim 4.25$, the commonly adopted dipole approximation of the Earth's mag-

netic field can be safely used for radiation belt electrons, while a realistic mod-

27 eling of the magnetic field configuration is necessary to describe adequately

28 the diffusion rates of ring current electrons.

1. Introduction

Resonant interaction between charged particles and plasma waves plays an important role in the description of energetic particle dynamics of the ring current and outer radiation belt [*Gendrin, R*, 2001; *Jordanova et al.*, 2001; *Shprits et al.*, 2008; *Thorne et al.*, 2005, 2010]. Wave-particle cyclotron resonance with wave frequency well below the particle gyrofrequency can cause pitch angle diffusion and lead to particle precipitation as particles enter into the atmosphere [*Jordanova et al.*, 2008]. Quasi-linear and nonlinear cyclotron resonance with EMIC waves has been suggested to account for the rapid loss of radiation belts electrons [*Lyons et al.*, 1972; *Bortnik et al.*, 2006; *Millan and Thorne*, 2007] and ring current ions [*Cornwall et al.*, 1970; *Jordanova et al.*, 2001; *Zhu et al.*, 2012; *Su et al.*, 2012]. On the other hand, wave-particle cyclotron resonance with wave frequency greater or comparable to the particle gyrofrequency, or wave-particle Landau resonance with any wave frequency, can induce significant energy diffusion [*Summers*, 2005]. Among the various waves that can lead to gyro-resonant wave-particle interaction, the whistler-mode chorus waves (often existing in two distinct frequency bands [Burtis and Helliwell, 1976] above and below one half of the local electron gyrofrequency) are an important candidate to drive electron acceleration. Recent studies provide observational evidence indicating that low energy particles can be accelerated to relativistic energies by chorus waves [*Horne et al.*, 2005a; *Shprits et al.*, 2006b; *Thorne et al.*, 2013]. Especially strong acceleration effects by chorus waves during nonstorm times were observed by Van Allen Probes [*Su et al.*, 2013, 2014], causing a potential threat to spacecraft and human activities in space. Thus, understanding the energetic particle dynamics is an essential task for

ring current and radiation belt research aimed at predicting the near-Earth environment and protecting space assets.

The standard model for energetic particle dynamics in the radiation belt stems from a Fokker-Planck diffusion equation in pitch angle, energy and drift shell coordinates. The pitch angle, energy and mixed term diffusion coefficients are normally estimated in the framework of quasi-linear theory. Historically, a general analysis of quasi-linear velocity space diffusion has been first given by [*Kennel and Engelmann*, 1966]. This general quasi-linear formulation is suitable for any modes of weak turbulence in a uniform, static magnetic field. Furthermore, an estimation of the diffusion coefficients resulting from gyro-resonant interaction of electrons with whistler waves was given by [*Lyons*, 1974a, b], where a Gaussian wave spectrum was specified. Summers [2005] derived a relativistic diffusion equation and calculated the diffusion coefficients for first order gyro-resonant interaction of particles with field-aligned whistler waves.

Starting from the Fokker-Planck equation and the related diffusion coefficients in a static magnetic field, bounce averaging can be performed in order to account for the magnetic field line geometry. This has been done by several authors in the context of a dipole approximation of the Earth's magnetic field [*Lyons et al.*, 1971, 1972; *Shprits et al.*, 2006; *Li et al.*, 2007]. However, recent work by Orlova and collaborators [*Orlova et al.*, 2010, 2012] compared bounce-averaged diffusion coefficients for a dipole magnetic field versus those obtained by the Tsyganenko 89c magnetic field model [*Tsyganenko et at.*, 1989] for quiet and stormy conditions. This work shows that the details of the magnetic field configuration can be quite different from a dipole during storms, resulting in significant differences

72 in the gyro-resonant diffusion coefficients. It also highlights the importance of the realistic

73 modeling of the magnetic field to calculate the diffusion coefficients accurately.

74 In this study, we perform an analysis of the role of the magnetic field geometry in

75 determining the pitch angle, energy and mixed diffusion rates for the March 17 2013 storm,

76 where the Van Allen Probes observed very rapid electron acceleration up to several MeV

77 within 12 hours [*Baker et al.*, 2014; *Li et al.*, 2014; *Xiao et al.*, 2014]. Unlike Orlova and

78 collaborators [*Orlova et al.*, 2010, 2012], the magnetic field geometry is obtained by the

79 ring current-atmosphere interactions model with a self-consistent magnetic field (RAM-

80 SCB) [*Jordanova et al.*, 2006, 2010; *Zaharia et al.*, 2006]. We investigate two geomagnetic

81 conditions, a) quiet (UT=4, prior to the storm) and b) stormy (UT=8, after storm onset).

82 RAM-SCB models the ring current population inside geosynchronous orbit and obtains

83 a more realistic magnetic field configuration self-consistently with the anisotropic plasma

84 pressure. Interestingly, our results show that, at least for the March 17 2013 storm, MLT-

85 and bounce-averaged diffusion coefficients (computed at $L = 4.25$, where MLT average is

86 a good approximation to drift average) for relativistic MeV electrons tend to be consistent

87 at three differents magnetic field geometries and a dipole field approximation can be safely

88 used. On the other hand, for electrons with lower energies (~ 100 keV) typical of the ring

89 current population, the details of the magnetic field are important and storm conditions

90 tend to enhance the diffusion rates at large equatorial pitch angles.

91 The paper is organized as follows. In section 2, we briefly discuss the RAM-SCB sim-

92 ulations and the quiet and stormy magnetic field configurations at $L = 4.25$ and $L = 6$

93 that are used in this study, together with a dipole field approximation. In section 3, we

94 introduce the bounce averaging procedure to calculate the pitch angle, momentum and

mixed diffusion coefficients along a general magnetic field line for whistler wave parallel propagation. We also discuss MLT average and drift average at $L = 4.25$. In section 4, we compare the bounce-averaged pitch angle diffusion coefficients at $L = 6$ and reproduce some of the results obtained by *Orlova et al.* [2010]. This comparison serves mostly as benchmark for our numerical procedure. In section 5, we compare the bounce-averaged diffusion coefficients at $L = 4.25$ for various electron energies, equatorial pitch angles and MLTs, and also perform MLT average. Conclusions are drawn in section 6.

2. Magnetic field configurations obtained from RAM-SCB

The kinetic ring current model RAM-SCB provides the external magnetic field, which is self-consistently computed in three dimensions with the anisotropic ring current plasma pressure. The internal magnetic field is obtained from the International Geomagnetic Reference Field (IGRF) model [*Maus et al.*, 2005]. The numerical tracing of magnetic field lines in the 3D magnetosphere domain follows the algorithm available in the Fortran library called International Radiation Belt Environment Modeling (IRBEM) library (http://sourceforge.net/projects/irbem/). With a particular equatorial pitch angle, we trace the magnetic field lines between two mirror points with a step resolution of 1/10,000 L, where L represents the distance of the point on the magnetic field line crossing the Earth's magnetic equator from the center of the Earth. Unlike empirical magnetic field models that directly provide the magnetic field intensity at any position, to obtain the RAM-SCB magnetic field at a particular location, we interpolate the magnetic field values from four neighboring grid points.

We simulate the magnetic storm event that occurred on March 17 2013 using the RAM-SCB model coupled with the global MHD code BATS-R-US [*Yu et al.*, 2014], to calculate

the inner magnetospheric configuration needed for the magnetic field tracing at points of

interest for this study. In this initial two-way coupling the MHD code provides plasma

boundary condition for RAM-SCB at geosynchronous orbit, while in return, the MHD

pressure in the inner magnetosphere region is specified by the RAM-SCB pressure. This

alters the global magnetospheric configuration and the field-aligned currents passed to the

ionospheric potential solver [*Ridley et al.*, 2004], which is used to provide the convection

electric field for the ring current particles. RAM-SCB is thus driven by a self-consistent

electric field in addition to its already existing self-consistent magnetic field.

The storm takes place around 6 UT when a CME-driven shock impacts on the mag-

netopause, leading to the rapid development of the ring current and the depression of

geomagnetic fields within a few hours. The storm main phase commences at ~ 6 UT,

reaches minimum ~ -100 nT at ~ 10 UT and the activity continues until ~ 20 UT when

the storm recovery phase begins. Fig. 1(a) shows an example of three magnetic field

tracings: the magnetic field line at $L = 4.25$ is plotted as a function of magnetic latitude

λ on the midnight local time (MLT=24) for storm time (red) at 8 UT and quiet time

(blue) at 4 UT during the above event. A dipole field line is shown in black for reference.

Similarly, three magnetic field tracings are plotted at different MLTs (e.g. MLT = 20,

16, 12, 8, 4) in Fig. 1(b), (c), (d), (e), (f), respectively). The mirror points correspond

to an equatorial pitch angle of $\alpha_{eq} = 30$ degree for this example. In general, we trace the

magnetic field line at different equatorial pitch angles from 5 degree to 87.5 degree with

2.5 degree apart. To compare the magnetic field models applied in *Orlova et al.* [2010],

we plot another three magnetic field tracings at L shell of 6 at MLT=24 in Fig. 2. Three

coordinates (x, y, z) describe the magnetic field geometry, with magnetic field latitude

given by $\lambda = \arctan\left(z/\sqrt{x^2 + y^2}\right)$. In the next sections, we will use these magnetic field configurations to calculate bounce- and MLT-averaged diffusion coefficients, with emphasis on the configuration at $L = 4.25$ where the wave spectrum parameters can be obtained from observation data from the Van Allen probes.

3. Calculation of bounce- and MLT-averaged diffusion coefficients

In the Earth's magnetic field, charged particles perform three types of motions: the gyro-motion around the magnetic field line, trapped motion along the magnetic field line where particles bounce back and forth between magnetic mirror points and drift motion around the Earth. There are three adiabatic invariants corresponding to each type of motion: magnetic moment, angular momentum and magnetic flux. Adiabatic invariance requires that the change of the magnetic field is much slower than the characteristic time of the particle motion. Thus, waves with frequency comparable to or exceeding the particle motion characteristic frequency will break the related adiabatic invariant and this can lead to particle diffusion. This is the case for whistler chorus, plasmaspheric hiss and electromagnetic ion cyclotron waves that can cause pitch angle scattering and energy diffusion via gyro-resonant wave-particle interaction. In particular, whistler-mode energy diffusion was able to produce realistic electron fluxes in the slot region for the 2003 Halloween storm [*Horne et al.*, 2005a; *Shprits et al.*, 2006b]. Lower ULF frequencies are instead responsible for radial (cross L) diffusion [*Ozeke et al.*, 2014; *Mathie et al.*, 2000; *Mann et al.*, 2012].

It is conventional to model the evolution of the distribution function of relativistic electrons in the framework of quasi-linear theory [*Kennel and Engelmann*, 1966]. For a

straight magnetic field configuration, this leads to a Fokker-Planck diffusion equation

$$\frac{\partial f}{\partial t} = \frac{1}{\sin\alpha}\frac{\partial}{\partial\alpha}\left(D_{\alpha\alpha}\sin\alpha\frac{\partial f}{\partial\alpha}\right) + \frac{1}{\sin\alpha}\frac{\partial}{\partial\alpha}\left(D_{\alpha p}\sin\alpha\frac{\partial f}{\partial p}\right) + \frac{1}{p^2}\frac{\partial}{\partial p}\left(p^2 D_{\alpha p}\frac{\partial f}{\partial\alpha}\right) + \frac{1}{p^2}\frac{\partial}{\partial p}\left(p^2 D_{pp}\frac{\partial f}{\partial p}\right)$$

(1)

written in terms of pitch angle α and relativistic momentum p, where $D_{\alpha\alpha}$, $D_{\alpha p}$ and

D_{pp} are diffusion coefficients. For first order gyro-resonant wave-particle interaction the

diffusion coefficients have been calculated by [*Summers*, 2005]. For whistler waves, one

has

$$D_{\alpha\alpha} = \frac{\pi}{2}\frac{1}{\nu}|\Omega_e|\frac{1}{(E_n+1)^2}\sum_{j=1}^{3}\frac{R\left(1 - \frac{x_j\cos\alpha}{y_j\beta}\right)^2|F(x_j,y_j)|}{\delta x|\beta\cos\alpha - F(x_j,y_j)|}e^{-\left(\frac{x_j - x_m}{\delta x}\right)^2}.$$

(2)

$$\frac{D_{\alpha p}}{p} = -\frac{\pi}{2}\frac{1}{\nu}|\Omega_e|\frac{\sin\alpha}{\beta(E_n+1)^2}\sum_{j=1}^{3}\frac{R\left(1 - \frac{x_j\cos\alpha}{y_j\beta}\right)|F(x_j,y_j)|}{\delta x|\beta\cos\alpha - F(x_j,y_j)|}\frac{x_j}{y_j}e^{-\left(\frac{x_j - x_m}{\delta x}\right)^2}.$$

(3)

$$\frac{D_{pp}}{p^2} = \frac{\pi}{2}\frac{1}{\nu}|\Omega_e|\frac{\sin^2\alpha}{\beta^2(E_n+1)^2}\sum_{j=1}^{3}\frac{R|F(x_j,y_j)|}{\delta x|\beta\cos\alpha - F(x_j,y_j)|}\left(\frac{x_j}{y_j}\right)^2 e^{-\left(\frac{x_j - x_m}{\delta x}\right)^2}.$$

(4)

where E_n is the dimensionless particle kinetic energy, $E_n = E/(m_e c^2)$ (E is the ki-

netic energy, m_e is the electron rest mass and c is the speed of light); $\beta = v/c =$

$[E_n(E_n + 2)]^{1/2}/(E_n + 1)$; $R = |\Delta B|^2/B_0^2$ is the ratio of the energy density of the

wave magnetic field to that of the background field $\mathbf{B}_0$; $x_m = \omega_m/|\Omega_e|$, $\delta x = \delta\omega/|\Omega_e|$,

$\nu = \sqrt{\pi}\text{erf}\left[(\omega_{uc} - \omega_{lc})/2\delta\omega\right]$, $|\Omega_e| = e|B_0|/(m_e c)$ is the electron gyrofrequency and

$F(x, y) = dx/dy$ is determined by the whistler mode wave dispersion relation

$$\frac{y^2}{x^2} = 1 - \left(\frac{\omega_{pe}}{\Omega_e}\right)^2\frac{1 + \epsilon}{(x - 1)(x + \epsilon)}.$$

(5)

where $\omega_{pe} = \sqrt{4\pi N_0 e^2/m_e}$ is the plasma frequency, $x = \omega/|\Omega_e|$, $y = ck/|\Omega_e|$, $\epsilon = m_e/m_p$

(m_p is the proton mass), ω is the wave frequency, k is wave number, and N_0 is the electron

density. Furthermore x_j and y_j satisfy the gyro-resonant condition

$$y = \frac{x - \dfrac{1}{\gamma}}{\beta\cos\alpha},$$

(6)

with $\gamma = 1/\sqrt{1 - \beta^2}$ the relativistic factor. In the derivation of Eqs. (2), (3) and (4), it is assumed that the wave power spectral density follows a Gaussian distribution peaked at ω_m with semi-bandwidth $\delta\omega$ and limited to the frequency band $\omega_{lc} \leq \omega \leq \omega_{uc}$, with $\omega_m = (\omega_{lc} + \omega_{uc})/2$ and $4\delta\omega = \omega_{uc} - \omega_{lc}$. Once the basic wave information (ω_m, $\delta\omega$, $|\Delta B|^2/B_0^2$) and particle parameters (α and E) are defined, the diffusion coefficients can be easily calculated via Eqs. (2), (3) and (4).

In order to account for a more realistic magnetic field geometry, the next step is to perform an average of the diffusion coefficients just discussed over the particle bounce motion between mirror points. For instance, the general pitch angle diffusion coefficient in a non-dipolar magnetic field has been given by Lyons (1971,1972).

$$\langle D_{\alpha\alpha}(\alpha_{eq})\rangle_{ba} = \frac{1}{\tau_b}\int_0^{\tau_b} D_{\alpha\alpha}(\alpha)\left(\frac{\partial\alpha_{eq}}{\partial\alpha}\right)^2 dt = \frac{2}{\tau_b v}\int_{s1}^{s2} D_{\alpha\alpha}(\alpha)\left(\frac{\partial\alpha_{eq}}{\partial\alpha}\right)^2 \frac{ds}{\cos\alpha}. \quad (7)$$

where subscript ba indicates bounce average and α_{eq} is the equatorial pitch angle of a particle, v is the magnitude of the particle velocity, $\tau_b = \frac{1}{v}\int_{s1}^{s2}\frac{ds}{\cos\alpha}$ is the electron bounce period and the temporal integral has been converted into an integral over the distance s along a given field line. For a general magnetic field line parametrized by $r(\lambda)$, the element of distance along a field line can be written as

$$ds = \sqrt{\left(\frac{\partial r}{\partial\lambda}\right)^2 + r^2}d\lambda, \quad (8)$$

leading to the following bounce-averaged diffusion coefficients:

$$\langle D_{\alpha\alpha}(\alpha_{eq})\rangle_{ba} = \frac{\int_{\lambda_1}^{\lambda_2} D_{\alpha\alpha}(\alpha,\lambda)\left(\frac{\tan\alpha_{eq}}{\tan\alpha(\lambda)}\right)^2 \sec\alpha(\lambda)\sqrt{\left(\frac{\partial r}{\partial\lambda}\right)^2 + r^2}d\lambda}{\int_{\lambda_1}^{\lambda_2} \sec\alpha(\lambda)\sqrt{\left(\frac{\partial r}{\partial\lambda}\right)^2 + r^2}d\lambda}, \quad (9)$$

$$\langle D_{pp}(\alpha_{eq})\rangle_{ba} = \frac{\int_{\lambda_1}^{\lambda_2} D_{pp}(\alpha,\lambda)\sec\alpha(\lambda)\sqrt{\left(\frac{\partial r}{\partial\lambda}\right)^2 + r^2}d\lambda}{\int_{\lambda_1}^{\lambda_2} \sec\alpha(\lambda)\sqrt{\left(\frac{\partial r}{\partial\lambda}\right)^2 + r^2}d\lambda}, \quad (10)$$

$$\langle D_{p\alpha}(\alpha_{eq})\rangle_{ba} = \langle D_{\alpha p}(\alpha_{eq})\rangle_{ba} = \frac{\int_{\lambda_1}^{\lambda_2} D_{p\alpha}(\alpha,\lambda)\frac{\tan\alpha_{eq}}{\tan\alpha(\lambda)}\sec\alpha(\lambda)\sqrt{\left(\frac{\partial r}{\partial\lambda}\right)^2 + r^2}d\lambda}{\int_{\lambda_1}^{\lambda_2}\sec\alpha(\lambda)\sqrt{\left(\frac{\partial r}{\partial\lambda}\right)^2 + r^2}d\lambda}, \qquad (11)$$

with λ_1 and λ_2 the magnetic latitudes corresponding to the two mirror points (north and

south side) on each magnetic field line. Note that the magnetic field is three dimensional

and we integrate the element of distance ds point by point along a field line in our numer-

ical calculation. In the following sections, we will use the magnetic field configurations

obtained numerically from RAM-SCB for the numerical evaluation of the bounce-averaged

diffusion coefficients given by Eqs. (9), (10) and (11). The bounce-averaged diffusion co-

efficients for a dipole field will be used to compare and contrast against those obtained

from the more realistic magnetic field geometry from RAM-SCB.

In addition to bounce average, we also perform MLT average, i.e. the arithmetic average

of the diffusion coefficients over the different MLTs. We do this only for the data at

$L = 4.25$ and note that in this case the MLT average is a good approximation to the drift

average, i.e. the average over the drift orbit, for both the quiet and storm inhomogeneous

magnetic field configurations considered in this paper. Indeed, we have traced electron

drift orbits in the magnetic field configuration corresponding to storm conditions (no

electric field) starting at $L = 4.25$ on the nightside (MLT=24) for various initial equatorial

pitch angles, following the procedure outlined in *Roederer and Zhang* [2014]. We find that

drift orbits are reasonably well approximated by a circle and that the change in equatorial

pitch angle during the orbit (to satisfy the conservation of magnetic moment) is quite

small. For instance, for initial $\alpha_{eq} = 10°, 50°, 80°$ the electron position on the dayside

(MLT=12) is $L \simeq 4.1, 4.3, 4.5$ (consistent with the results of *Roederer and Zhang* [2014])

and the maximum change in equatorial pitch angle over the orbit is $\Delta\alpha_{eq} < 3°, 8°, 3°$.

227 These results indicate that MLT average and drift average are reasonably close in this

228 case. Of course, the two are exactly equivalent in the case of a dipole field.

4. Benchmarking our numerical procedure: Calculation of $D_{\alpha\alpha}$ at $L = 6$

229   In this section we will discuss the numerical results for the calculation of the bounce-

230 averaged diffusion coefficients for the three magnetic field configurations corresponding to

231 $L = 6$ (shown in Fig. 2). This case was analyzed in *Orlova et al.* [2010], where the effect

232 of the magnetic field geometry on the diffusion rates was investigated. Specifically, *Orlova*

233 *et al.* [2010] compared a dipole magnetic field with a magnetic field configuration given by

234 the Tsyganenko 89c model [*Tsyganenko et at.*, 1989] for quiet ($K_p = 2$) and storm-time

235 ($K_p = 6$) conditions. These results will serve as benchmark for our numerical solution of

236 Eq. (9). In Sec. 5 we will extend the calculation of the diffusion coefficients (including

237 energy and mixed terms) at $L = 4.25$, where the wave parameters are different.

238   We use the statistical trough plasma density model [*Sheeley et al.*, 2001] and assume that

239 plasma density is constant along the field line based on the statistical study of *Denton et al.*

240 [2006]. The wave frequency parameters are dependent on the equatorial gyrofrequency

241 Ω_{eq}, consistent with observations indicating that chorus waves are generated near the

242 equator. The wave spectrum parameters (on the nightside) are taken as $\omega_m = 0.35\Omega_{eq}$,

243 $\delta\omega = 0.15\Omega_{eq}$, $\omega_{lc} = 0.05\Omega_{eq}$ and $\omega_{uc} = 0.65\Omega_{eq}$ following *Horne et al.* [2005]. In addition,

244 we assume that the whistler waves are confined to magnetic latitude $|\lambda| < 15°$ from the

245 magnetic equator [*Horne et al.*, 2005; *Li et al.*, 2007; *Orlova et al.*, 2010]. The wave

246 amplitude is assumed constant for all magnetic latitudes, with $\Delta B = 100$ pT. Finally, we

247 consider the interaction of whistler waves with relativistic electrons with energy $E = 1$

248 MeV.

By inserting the above wave and particle parameters into Eq. (2), we obtain the local pitch angle diffusion coefficient $D_{\alpha\alpha}$ and then calculate its bounce average through Eq. (9) for the dipole and the non-dipolar magnetic field configurations, respectively. For convenience, in the following we will use the terms 'RAM-SCB quiet' and 'RAM-SCB storm' to refer to the (non-dipolar) magnetic field configurations obtained from RAM-SCB prior (UT=4) and after (UT=8) the storm onset. In Fig 3, we plot the bounce-averaged pitch angle diffusion coefficient as a function of equatorial pitch angle. The black, blue and red lines correspond to the dipole field, RAM-SCB quiet and RAM-SCB storm respectively, all for MLT=24. The dipole magnetic field approximation leads to a non-zero diffusion coefficient only between $52° < \alpha_{eq} < 90°$, while for RAM-SCB quiet this occurs for $27° < \alpha_{eq} < 90°$. RAM-SCB storm leads to a non-zero $\langle D_{\alpha\alpha}(\alpha_{eq})\rangle_{ba}$ for the whole interval considered in Fig. 3, i.e. $5° < \alpha_{eq} < 90°$. One can see that the bounce-averaged diffusion coefficient for RAM-SCB storm dominates at small equatorial pitch angles $\alpha_{eq} < 40°$. On the other hand, at intermediate equatorial pitch angles $40° < \alpha_{eq} < 60°$, $< D_{\alpha\alpha}(\alpha_{eq}) >_{ba}$ is bigger for RAM-SCB quiet. At large pitch angles $60° < \alpha_{eq} < 85°$, the dipole field produces the largest $< D_{\alpha\alpha(\alpha_{eq})} >_{ba}$, although all three cases converge to similar values when the equatorial pitch angle is near $90°$. These results are very similar to those of Fig. 1 in *Orlova et al.* [2010] where the calculation of the bounce-averaged pitchangle diffusion coefficients were based on a Tsyganenko 89 model. This is not surprising, since RAM-SCB uses the Tsyganenko 89 model as boundary condition for the magnetic field at the geosynchronous ($L = 6.6$) orbit for this simulation. They also confirm the importance of the magnetic field geometry in determining the diffusion rates, relative to the commonly adopted dipole field approximation.

In order to understand the differences in scattering rates for these three magnetic field configurations, we follow [*Orlova et al.*, 2010] and plot in Fig. 4 the local diffusion rates as function of latitude along the magnetic field line for each model in Fig. 2. In this figure the wave field is present at all latitudes (i.e. it is not limited to $|\lambda| < 15°$) and we vary the equatorial pitch angle between $5° < \alpha_{eq} < 85°$. In general, for each α_{eq} diffusion occurs mostly at larger latitudes and over a rather narrow latitude range. Comparing the different plots in Fig. 4, one can see the latitude range where wave-particle resonance (hence diffusion) occurs: for the dipole field the largest latitude range is between $-39° < \lambda < 39°$, while we have $-32° < \lambda < 32°$ for RAM-SCB quiet and $-22° < \lambda < 22°$ for RAM-SCB storm. From Fig. 4(a), it is easy to see why resonant diffusion occurs only for $\alpha_{eq} > 50°$ for the dipole field when the wave field is limited to $|\lambda| < 15°$: when $\alpha_{eq} < 50°$ wave-particle resonances occur only at larger latitudes, where the wave field is zero. Similarly, resonant diffusions occur only for $\alpha_{eq} > 30°$ for quiet conditions [Fig. 4(b)] and for $\alpha_{eq} > 5°$ for storm conditions [Fig. 4(c)] when the wave field is limited to $|\lambda| < 15°$. These results on the local wave-particle resonance are consistent with the bounce-averaged wave-particle resonance shown in Fig. 3. In addition, Fig. 4(b) and Fig. 4(c) we note that the local diffusion coefficients show some north-south asymmetry in quiet and storm conditions. This is a consequence of the magnetic field lines described by RAM-SCB, which can be not symmetric in quiet and storm conditions. This asymmetry is more evident at larger equatorial pitch angles.

5. Calculation of the bounce- and MLT-averaged diffusion coefficients $D_{\alpha\alpha}$, $D_{\alpha p}$ and D_{pp} at $L = 4.25$

5.1. Calculation of bounce-averaged pitch angle diffusion coefficients $\langle D_{\alpha\alpha}(\alpha_{eq})\rangle_{ba}$ at $L = 4.25$

292   In order to compare with the results at $L = 6$, we begin by calculating the bounce-

293   averaged pitch angle diffusion coefficient at $L = 4.25$. The parameters of whistler waves

294   and plasma at different MLT are listed in Table 1. We have adapted these from the global

295   chorus wave model developed by *Li et al.* [2014] based on direct observations from the

296   EMFISIS instrument on the Van Allen Probes and inferred from POES measurements.

297   In Table 1, $|\lambda|$ is the wave latitudinal extension where the chorus waves are confined, n_e

298   is the electron density, and we choose an average chorus wave amplitude $\langle B_w \rangle = 100$ pT

299   for all MLTs.

300   For each of the three magnetic field configurations shown for various MLTs (e.g. MLT

301    $= 24, 20, 16, 12, 8$ and 4) in Fig. 1, we insert the wave and density parameters into Eq.

302   (9) and obtain the bounce-averaged pitch angle diffusion coefficients $\langle D_{\alpha\alpha} \rangle_{ba}$ at $L = 4.25$

303   for each MLT. The diffusion coefficients are plotted in Figs. 5 and 6, for electron energy

304    $E = 1$ MeV and $E = 100$ keV, respectively, as a function of equatorial pitch angle α_{eq}.

305   For $E = 1$ MeV, we note that $\langle D_{\alpha\alpha} \rangle_{ba}$ at nightside MLT $= 24, 20, 4$ [Fig. 5(a), (b), (f)]

306   have big differences at low and intermediate equatorial pitch angles, similarly to what has

307   been discussed for $L = 6$. On the other hand, the values of $\langle D_{\alpha\alpha} \rangle_{ba}$ at dayside MLT $=$

308   16, 12, 8 [Fig. 5(c), (d), (e)] are almost the same for all the magnetic field configurations

309   that were considered. Note also that for $\alpha_{eq} < 40°$, $\langle D_{\alpha\alpha} \rangle_{ba}$ is orders of magnitude larger

310   at MLT=12 and MLT=16 than at other MLTs.

311   The case for electron energy $E = 100$ keV plotted in Fig. 6 shows some differences

312   relative to $E = 1$ MeV. For dayside MLT=16, 12 and 8, there is a reasonable agreement

313 on $\langle D_{\alpha\alpha} \rangle_{ba}$ for all magnetic field configurations except that the bounce-averaged pitch

314 angle diffusion coefficient for storm conditions can be up to a factor of three larger than

315 that for a dipole at larger equatorial pitch angles. For nightside MLT=24, 20 and 4, one

316 can notice large discrepancy at large α_{eq}: for storm conditions the range of equatorial

317 pitch angles with non-zero $\langle D_{\alpha\alpha} \rangle_{ba}$ widens, and there is a range of α_{eq} where the value

318 of $\langle D_{\alpha\alpha} \rangle_{ba}$ can be an order of magnitude higher than that for a dipole field. In general,

319 the values of $\langle D_{\alpha\alpha} \rangle_{ba}$ are much larger for $E = 100$ keV than for relativistic electrons with

320 $E = 1$ MeV for all MLTs at $\alpha_{eq} < 60°$.

5.2. Calculation of the MLT-averaged diffusion coefficients $D_{\alpha\alpha}$, $D_{\alpha p}$ and D_{pp}

321 Next, we perform MLT average of $\langle D_{\alpha\alpha} \rangle_{ba}$ and plot the results in Fig. 7 for electron en-

322 ergies $E = 100$ keV and $E = 1$ MeV. We recall that MLT average is a good approximation

323 to drift average at $L = 4.25$, as discussed in Sec. 3.

324 For $E = 1$ MeV, Fig. 7 (b) shows that the MLT-averaged pitch angle diffusion coef-

325 ficient is quite independent on the magnetic field configuration. This is because at large

326 equatorial pitch angles all the magnetic field configurations produce rather similar values

327 of $\langle D_{\alpha\alpha} \rangle_{ba}$, while at low equatorial pitch angles the drift average is dominated by the

328 values at MLT=12 and 16 (see Fig. 5). Thus, for relativistic particles the effect of the

329 magnetic field geometry is limited and the dipole field approximation adopted for instance

330 in *Li et al.* [2014] is a good approximation. On the other hand, Fig. 7 (a) shows that

331 the details of the magnetic field configuration are very important for particles with lower

332 energy, even after MLT-averaging. For $E = 100$ keV, one can see that storm conditions

333 lead to a wider range of pitch angle scattering and that the MLT-averaged diffusion co-

334 efficient in storm conditions is at least a factor of three larger than that obtained for the

dipole field when $\alpha_{eq} > 60°$. Thus, for the lower energy particle typical of the ring current

population, the dipole field approximation can be inadequate.

We now extend the calculation of the diffusion coefficients to mixed and momentum

diffusion terms. We use the same parameters in Table 1 and perform MLT average of

Eqs. (10) and (11). Figures 8 and 9 show the MLT-averaged mixed and momentum

diffusion coefficients for electrons with energy $E = 100$ keV and $E = 1$ MeV, respectively.

The same trend of Fig. 7 also occurs in Figs. 8 and 9: for $E = 1$ MeV electrons, the

diffusion coefficient is rather insensitive to the details of the magnetic field configuration.

On the other hand, for $E = 100$ keV diffusion is enhanced in storm conditions and there

are big differences (above a factor of three) relative to the dipole configuration at large

equatorial pitch angles $65° < \alpha_{eq} < 80°$.

Figures 10 show pitch angle, momentum and mixed term diffusion coefficients as a

function of the equatorial pitch angle α_{eq} and the electron kinetic energy E from 100 keV to

10 MeV for the dipole configuration, RAM-SCB storm and RAM-SCB quiet, respectively.

Although it is somewhat hard to discern the detailed differences of the three figures, in

general the diffusion coefficients peak at intermediate equatorial pitch angles ($40° < \alpha_{eq} <$

$60°$) over the energy range considered. In addition, for energy above 1 MeV, the diffusion

coefficients are very similar for the three magnetic field configurations. However, at lower

energy range 100 keV$\leq E <$1 MeV, the diffusion coefficients show significant differences,

with resonant diffusion occurring at higher equatorial pitch angles in storm conditions

relative to the other two cases. Comparing the three diffusion coefficients, one can see

that the pitch angle scattering rate is the biggest while the momentum diffusion coefficient

is the smallest. The cross term diffusion coefficients are bigger or at least comparable to the momentum ones and can contribute to energy diffusion as well.

In our calculation, we assumed the whistler wave propagation along the magnetic field line up to $|\lambda| = 15$ degree. Only the first order cyclotron wave-particle resonances ($n = \pm 1$) were considered. However, for oblique whistler wave-particle resonance, higher resonant harmonics ($n = \pm 2, \pm 3, \pm 4 \ldots$) also need to be considered. This case has been discussed in *Orlova et al.* [2012], which studied on resonant interactions of the outer radiation belt electrons with oblique chorus waves in a realistic magnetic field model (here the Tsyganenko 2001 storm field model and an internal IGRF model are choosen as realistic field models in storm and quiet conditions). They showed that higher resonant harmonic significantly contribute to diffusion coefficients in all three field models on both dayside and nightside at the intermediate equatorial pitch angles. In addition, they stated that the bounce-averaged diffusion coefficients are indistinguishable for all three field models for energies E $\leq$ 1 MeV at the dayside. On the nightside at L = 7, the bounce-averaged scattering computed in the dipole field and those computed in the realistic magnetic fields can differ by several orders of magnitude. Extension of our procedure to oblique whistler waves is left for future work.

Finally we conclude this section with a brief discussion of how the bounce-averaged pitch angle diffusion coefficients change with wave intensity and plasma density assuming a fixed magnetic field geometry corresponding to quiet, storm and dipole magnetic field configurations that we obtained before at $L = 4.25$ and MLT=24. We focus on $E = 1$ MeV particles. First of all, the wave intensity enters the formulation of the problem only through the coefficient R in Eqs. (2)-(4). It is a quadratic dependence, meaning that if

the amplitude of the wave-field doubles the diffusion coefficients increase by a factor of 4. Most important, the effects of the wave-field intensity and of magnetic field geometry are *indepedent*, therefore the considerations that we made in Secs. 4 and 5 remain completely valid. Next, we look at how the bounce-averaged diffusion coefficients vary with electron density, keeping the other parameters fixed (in particular the wave amplitude is 100 pT). We anticipate a more complex dependence of the diffusion coefficients, since the plasma density enters the whistler wave dispersion relation Eq. (5) non-linearly, and have therefore calculated it numerically. The results are plotted in Fig. 11, where the electron density changes from $6.55 \times 10^6 m^{-3}$ to $1.31 \times 10^8 m^{-3}$. In general, the diffusion coefficients decrease with higher electron density monotonically. Although increasing or decreasing the density changes the diffusion coefficients by a factor of order unity, the same trend discussed in Secs. 4 and 5 remains visible in Fig. 11 and the magnetic field geometry can expand the range of equatorial pitch angles where resonant diffusion occurs. Thus, the magnetic field geometry is as important as the wave-amplitude and the background plasma density in controlling the level of resonant diffusion.

6. Conclusions

In this paper we have analyzed the role played by a more realistic magnetic field configuration in determining MLT- and bounce-averaged quasi-linear diffusion rates for gyro-resonant interaction of inner magnetospheric electrons with field-aligned whistler chorus waves. In particular, we have focused on the March 17 2013 storm. We modeled this storm with the RAM-SCB ring current code coupled with the BATS-R-US global magnetosphere code. RAM-SCB provides the self-consistent modeling of the magnetic field with the anisotropic plasma pressure and offers a more realistic magnetic field configuration

during storms than empirical models. We have selected two magnetic field configurations from RAM-SCB: the first is for quiet conditions prior to the storm (UT=4) and the other is for storm conditions after its onset (UT=8). Both configurations have been compared against a dipole approximation of the Earth's magnetic field which has been adopted in several past studies. The parameters for whistler waves and plasma needed for the calculation of the diffusion coefficients are obtained after measurements from the Van Allen Probes.

We have compared bounce-averaged pitch angle diffusion coefficients for the three magnetic field configurations at $L = 6$. Essentially we have reproduced some of the results of *Orlova et al.* [2010], thus verifying our numerical procedure for calculating bounce-averaged diffusion coefficients.

We have then focused on the comparison at $L = 4.25$, analyzing gyro-resonant diffusion for 100 keV and 1 MeV electrons at various MLTs. For bounce-averaged pitch angle diffusion, both energies exhibit ranges in MLT ($\simeq 8 - 16$, dayside) where storm, quiet and dipole magnetic field configurations produce rather similar (within a factor of two) rates, and ranges (MLT$\simeq 20 - 4$, nightside) where there are significant differences due to differences in the magnetic field configuration. The latter are both in terms of the range in equatorial pitch angle where resonant diffusion can occur and in terms of magnitude of the diffusion coefficient (with discrepancies up to a factor five-ten). Specifically, for 1 MeV electrons, storm conditions favor pitch angle scattering at low values of the equatorial pitch angle, while the opposite is true for 100 keV electrons. However, we show that when MLT average is performed (which, at $L = 4.25$, is a good approximation to drift average), pitch angle scattering becomes insensitive to the magnetic field configuration

for relativistic electron energies. This is not the case for lower electron energy, where the MLT-averaged pitch angle diffusion coefficients maintain that storm conditions enhance pitch angle scattering at large equatorial pitch angles. Similar trends also occur for mixed and momentum diffusion coefficients, although these coefficients are comparatively smaller than $D_{\alpha\alpha}$.

Our results suggest that, at least for the March 17 2013 storm and $L \lesssim 4.25$, a dipole approximation of the Earth's magnetic field can be safely adopted for the modeling of relativistic MeV electrons. Such approximation, however, is inadequate for ring current electrons in the 100 keV range and a realistic magnetic field model is required. Future work will study how these differences in diffusion coefficients induced by a realistic modeling of the magnetic field translate into electron fluxes for the ring current and radiation belt.

References

Baker, D. N., and S. G. Kanekal (2008), Solar cycle changes, geomagnetic variations, andenergetic particle properties in the inner magnetosphere, *J. Atmos. Sol. Terr. Phys.*, *70*, 195206.

445 Baker, D. N., et al. (2014), Gradual diffusion and punctuated phase space density en-

446   hancements of highly relativistic electrons: Van Allen Probes observations, *Geophys.*

447   *Res. Lett.*, *41*, 13511358, doi:10.1002/2013GL058942.

448 Bortnik, J., R. M. Thorne, T. P. OBrien, J. C. Green, R. J. Strangeway, Y. Y. Shprits,

449   and D. N. Baker (2006), Observation of two distinct, rapid loss mechanisms during

450   the 20 November 2003 radiation belt dropout event, *J. Geophys. Res.*, *111*, A12216,

451   doi:10.1029/2006JA011802.

452 Cornwall, J. M., F. V. Coroniti, and R. M. Thorne (1970), Turbulent loss of ring current

453   protons, *J. Geophys. Res.*, *75*, 46994709, doi:10.1029/ JA075i025p04699.

454 Denton, R. E., K. Takahashi, I. A. Galkin, P. A. Nsumei, X. Huang, B. W. Reinisch, R.

455   R. Anderson, M. K. Sleeper, and W. J. Hughes (2006), Distribution of density along

456   magnetospheric field lines, *J. Geophys. Res.*, *111*, A04213, doi:10.1029/ 2005JA011414.

457 Gendrin, R. (2001), The role of wave particle interactions in radiation belts modeling,

458   *Sun-Earth Connection and Space Weather*, vol. 75, edited by M. Candidi, M. Storini,

459   and U. Villante, p. 151, SIF, Bologna.

460 Horne, R. B., and R. M. Thorne (2003), Relativistic electron acceleration and precipitation

461   during resonant interactions with whistler-mode chorus, *Geophys. Res., Lett.*, *30*(10),

462   1527, doi:10.1029/2003GL016973.

463 Horne, R. B., R. M. Thorne, S. A. Glauert, J. M. Albert, N. P. Meredith, and R. R.

464   Anderson (2005), Timescale for radiation belt electron acceleration by whistler mode

465   chorus waves, *J. Geophys. Res.*, *110*, A03225, doi:10.1029/2004JA010811.

466 Horne, R. B., et al. (2005a), Wave acceleration of electrons in the Van Allen radiation

467   belts, *Nature*, *437*, 227230, doi:10.1038/nature03939.

Jordanova, V. K., C. J. Farrugia, R. M. Thorne, G. V. Khazanov, G. D. Reeves, and M. F. Thomsen (2001), Modeling ring current proton precipitation by electromagnetic ion cyclotron waves during the May 1416, 1997, storm, *J. Geophys. Res.*, *106(A1)*, 722, doi:10.1029/2000JA002008.

Jordanova, V. K., Y. S. Miyoshi, S. Zaharia, M. F. Thomsen, G. D. Reeves, D. S. Evans, C. G. Mouikis, and J. F. Fennell (2006), Kinetic simulations of ring current evolution during the Geospace Environment Modeling challenge events, *J. Geophys. Res.*, *111*, A11S10, doi:10.1029/2006JA011644.

Jordanova, V. K., J. Albert, and Y. Miyoshi (2008), Relativistic electron precipitation by EMIC waves from self-consistent global simulations, *J. Geophys. Res.*, *113*, A00A10, doi:10.1029/2008JA013239.

Jordanova, V. K., S. Zaharia, and D. T.Welling (2010), Comparative study of ring current 380 development using empirical, dipolar, and self-consistent magnetic field simulations, *J. 381 Geophys. Res.*, *115*, A00J11, doi:10.1029/2010JA015671.

Kennel, C. F., and F. Engelmann (1966), Velocity space diffusion from weak plasma turbulence in a magnetic fields, *Phys. Fluids*, *9*, 2377-2388.

Li, W., Y. Y. Shprits, and R. M. Thorne (2007), Dynamic evolution of energetic outer zone electrons due to wave-particle interactions during storms, *J. Geophys. Res.*, *112*, A10220, doi:10.1029/2007JA012368.

Li, W., et al. (2014), Radiation belt electron acceleration by chorus waves during the 17 March 2013 storm, *J. Geophys. Res. Space Physics*, *119*, 46814693, doi:10.1002/2014JA019945.

Lyons, L. R. (1974a), General relations for resonant particle diffusion in pitch angle and energy, *J. Plasma Phys.*, *12*, 45

Lyons, L. R. (1974b), Pitch angle and energy diffusion coefficients from resonant interactions with ion-cyclotron and whistler waves, *J. Plasma Phys.*, *12*, 417.

Lyons, L. R., R. M. Thorne, and C. F. Kennel (1972), Pitch-angle diffusion of radiation belt electrons within the plasmasphere, *J. Geophys. Res*, *77*, 3455-3474,doi:10.1029/JA077i019p03455.

Lyons, L. R., R. M. Thorne, and C. F. Kennel (1971), Electron pitch-angle diffusion driven by oblique whistler mode turbulence, *J. Plasma Phys.*, *6*, 589606.

Mann, I. R., K. R. Murphy, L. G. Ozeke, I. J. Rae, D. K. Milling, A. Kale, and F. Honary (2012), The role of ultralow frequency waves in radiation belt dynamics, *Geophys. Monogr. Ser.*, *199*, 6991.

Millan, R. M., and R. M. Thorne (2007), Review of radiation belt relativistic electron losses, *J. Atmos. Sol. Terr. Phys.*, *69*, 362377, doi:10.1016/ j.jastp.2006.06.019.

Maus, S., S. MacMillan, T. Chernova, S. Choi, D. Dater, V. Golovkov, V. Lesur, F. Lowes, H. Lühr, W. Mai, S. McLean, N. Olsen, M. Rother, T. Sabaka, A. Thomson, and T. Zvereva, T.Baker (2005), The 10th generation international geomagnetic reference field, *Physics of the Earth and Planetary Interiors*, *151*, 320-322.

Mathie, R., and I. Mann (2000), A correlation between extended intervals of ULF wave power and storm-time geosynchronous relativistic electron flux enhancements, *Geophys. Res. Lett.*, *27*, 32613264, doi:10.1029/2000GL003822

Perry, K. L., M. K. Hudson, and S. R. Elkington (2005), Incorporating spectral characteristics of Pc5 waves into three-dimensional radiation belt modeling and the diffusion

513   of relativistic electrons, *J. Geophys. Res.*, *110*, A03215, doi:10.1029/2004JA010760.

514   Orlova, K. G. and Y. Y. Shprits (2010), Dependence of pitch-angle scattering rates

515   and loss timescales on the magnetic field model, *Geophys. Res. Lett.*, *37*, L05105,

516   doi:10.1029/2009GL041639

517   Orlova, K. G. and Y. Y. Shprits (2011), On the bounce-averaging of scattering rates and

518   the calculation of bounce period, *Phys. Plasmas*, *18*, 092904, doi:10.1063/1.363813.

519   Orlova, K. G., Y. Y. Shprits, and B. Ni (2012), Bounce-averaged diffusion coefficients

520   due to resonant interaction of the outer radiation belt electrons with oblique chorus

521   waves computed in a realistic magnetic field model, *J. Geophys. Res.*, *117*, A07209,

522   doi:10.1029/2012JA017591.

523   Ozeke, L. G., I. R. Mann, D. L. Turner,K. R. Murphy, A. W. Degeling, I. J. Rae,

524   and D. K. Milling (2014), Modeling cross L shell impacts of magnetopause shadow-

525   ing and ULF wave radial diffusion in the Van Allen belts, *Geophys. Res. Lett.*, *41*,

526   doi:10.1002/2014GL060787

527   Ridley, A., T. Gombosi, and D. Dezeeuw (2004), Ionospheric control of the magnetosphere:

528   Conductance, *Ann. Geophys.*, *22*, 567584, doi:10.5194/angeo-22-567-2004.

529   Roederer, J. G., and Hui Zhang, Dynamics of Magnetically Trapped Particles, *Astro-*

530   *physics and Space Science Library*. Vol. 403. 2014.

531   Sheeley, B. W., M. B. Moldwin, H. K. Rassoul, and R. R. Anderson (2001), An empir-

532   ical plasmasphere and trough density model: CRRES observations, *J. Geophys. Res.*,

533   *106(A11)*, 2563125641, doi:10.1029/2000JA000286.

534   Shprits, Y. Y., R. M. Thorne, R. B. Horne, and D. Summers (2006), Bounce-averaged

535   diffusion coefficients for field-aligned chorus waves, *Geophys. Res. Lett.*, *111*, A10225,

doi:10.1029/2006JA011725.

Shprits, Y. Y., R. M. Thorne, R. B. Horne, S. A. Glauert, M. Cartwright, C. T. Russell, D. N. Baker, and S. G. Kanekal (2006b), Acceleration mechanism responsible for the formation of the new radiation belt during the 2003 Halloween solar storm, *Geophys. Res. Lett.*, *33*, L05104, doi:10.1029/2005GL024256.

Shprits, Y. Y., D. A. Subbotin, N. P. Meredith, and S. R. Elkington (2008), Review of modeling of losses and sources of relativistic electrons in the outer radiation belt II: Local acceleration and loss, *J. Atmos. Sol. Terr. Phys.*, *70*, 16941713, doi:10.1016/j.jastp.2008.06.014.

Shprits, Y. Y., and B. Ni (2009), Dependence of the quasi-linear scattering rates on the wave normal distribution of chorus waves, *J. Geophys. Res.*, *114*, A11205, doi:10.1029/2009JA014223.

Su, Z., H. Zhu, F. Xiao, H. Zheng, C. Shen, Y. Wang, and S. Wang (2012), Bounce-averaged advection and diffusion coefficients for monochromatic electromagnetic ion cyclotron wave: Comparison between test-particle and quasi-linear models, *J. Geophys. Res.*, *117*, A09222, doi:10.1029/2012JA017917.

Su, Z., et al. (2014), Nonstorm time dynamics of electron radiation belts observed by the Van Allen Probes, *Geophys. Res. Lett.*, *41*, 229235, doi:10.1002/2013GL058912.

Su, Z., et al. (2014), Intense duskside lower band chorus waves observed by Van Allen Probes: Generation and potential acceleration effect on radiation belt electrons, *J. Geophys. Res. Space Physics*, *119*, 42664273, doi:10.1002/2014JA019919.

Summers, D., C. Ma, N. P. Meredith, R. B. Horne, R. M. Thorne, D. Heynderickx, and R. R. Anderson (2002), Model of the energization of outer-zone electrons by whistler-mode

559   chorus during the October 9, 1990 geomagnetic storm, *Geophys. Res. Lett.*, *29*(24),2174,

560   doi:10.1029/2002GL016039.

561   Summers, D. (2005), Quasi-linear diffusion coefficients for field-aligned electromag-

562   netic waves with applications to the magnetosphere, *J. Geophys. Res.*, *110*, A08213,

563   doi:10.1029/2005JA011159.

564   Summers, D., and R. M. Thorne (2003), Relativistic electron pitch-angle scattering by

565   electromagnetic ion cyclotron waves during geomagnetic storms, *J. Geophys. Res.*,

566   *108*(A4), 1143, doi:10.1029/2002JA009489.

567   Thorne, R. M., R. B. Horne, S. A. Glauert, N. P. Meredith, Y. Shprits, D. Summers, and R.

568   R. Anderson (2005), The Influence of Wave-Particle Interactions on Relativistic Electron

569   Dynamics During Storms, in Inner Magnetosphere Interactions: New Perspectives from

570   Imaging, edited by J. Burch, M. Schulz and H. Spence, *American Geophysical Union*,

571   Washington, D. C., doi: 10.1029/159GM07

572   Thorne, R. M., et al. (2010), Scattering by chorus waves as the dominant cause of diffuse

573   auroral precipitation, *Nature*, *467*, 943946, doi:10.1038/nature09467.

574   Thorne, R. M., et al. (2013), Rapid local acceleration of relativistic radiation belt electrons

575   by magnetospheric chorus, *Nature*, *504*, 7480, doi:10.1038/nature12889.

576   Tsyganenko, N. A. (1989), A magnetospheric magnetic field model with a wraped tail

577   current sheet, *Planet. Space Sci.*, *37*, 5-20.

578   Ukhorskiy, A. Y., M. I. Sitnov, K. Takahashi, and B. J. Anderson (2009), Radial transport

579   of radiation belt electrons due to stormtime Pc5 waves, *Ann. Geophys.*, *27*, 21732181.

580   Xiao, F., et al. (2014), Chorus acceleration of radiation belt relativistic electrons dur-

581   ing March 2013 geomagnetic storm, *J. Geophys. Res. Space Physics*, *119*, 33253332,

582   doi:10.1002/2014JA019822.

583   Yu, Y., V. Jordanova, D. Welling, B. Larsen, S. G. Claudepierre, and C. Kletzing

584   (2014), The role of ring current particle injections: Global simulations and Van Allen

585   Probes observations during 17 March 2013 storm, *Geophys. Res. Lett.*, *41*, 11261132,

586   doi:10.1002/2014GL059322.

587   Zaharia, S., V. K. Jordanova, M. F. Thomsen, and G. D. Reeves (2006), Self-consistent

588   modeling of magnetic fields and plasmas in the inner magnetosphere: Application to a

589   geomagnetic storm, *J. Geophys. Res.*, *111*, A11S14, doi:10.1029/2006JA011619.

590   Zhu, H., Z. Su, F. Xiao, H. Zheng, C. Shen, Y. Wang, and S. Wang (2012), Nonlinear

591   interaction between ring current protons and electromagnetic ion cyclotron waves, *J.*

592   *Geophys. Res.*, *117*, A12217, doi:10.1029/2012JA018088.
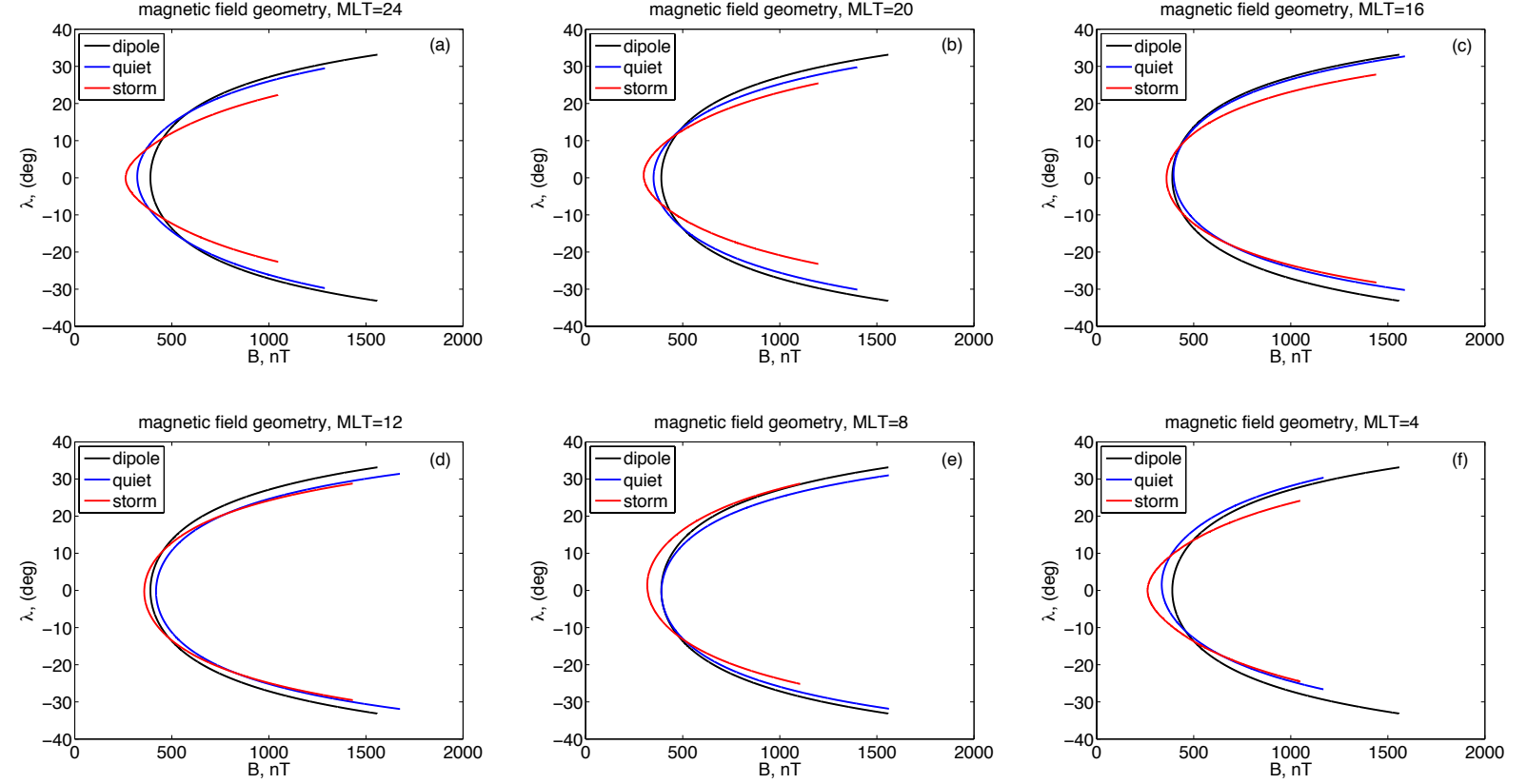
Figure 1.   Magnetic field magnitude along the field line versus magnetic latitude at $L = 4.25$ obtained by RAM-SCB modeling of the 17 March 2013 storm for nightside storm (red line, UT=8) and quiet (blue line, UT=4) conditions. A dipole magnetic field is also plotted (black line). The mirror points correspond to an equatorial pitch angle of $\alpha_{eq} = 30$ degree. Figures (a) to (e) correspond to MLT= 24, 20, 16, 12, 08, 04, respectively.
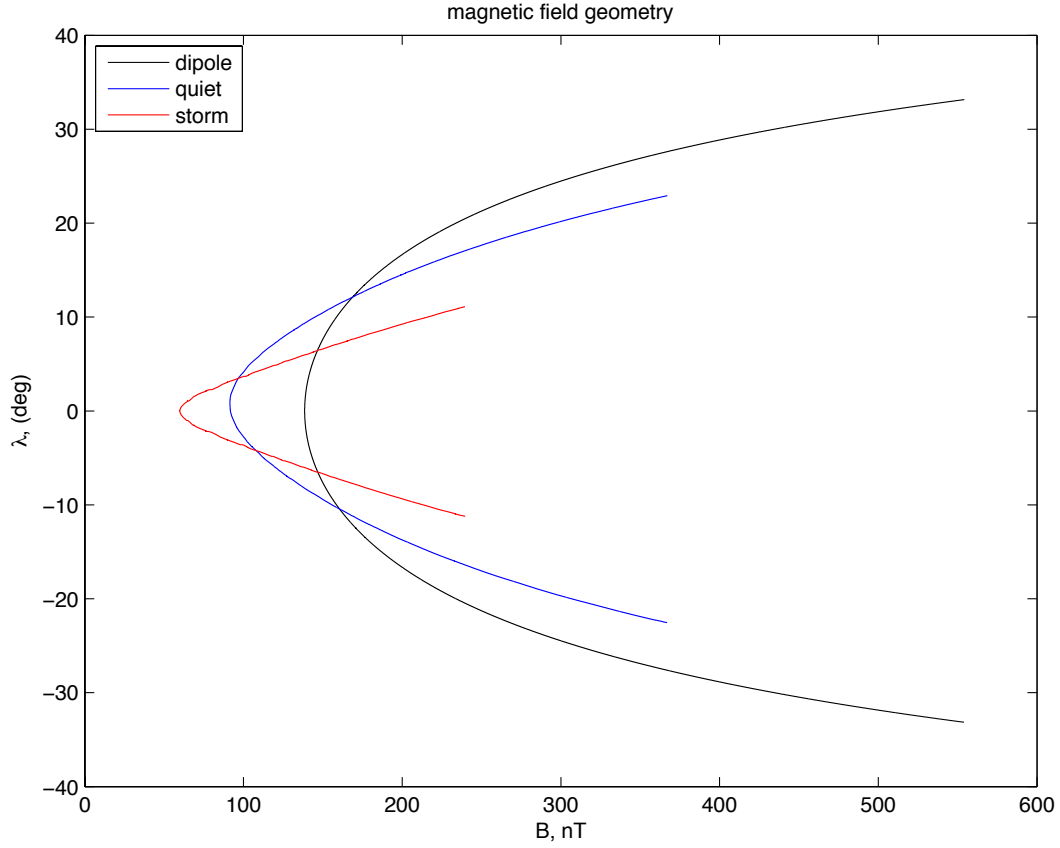
Figure 2. Magnetic field magnitude along the field line versus magnetic latitude at $L = 6$ obtained by RAM-SCB modeling of the 17 March 2013 storm for nightside storm (red line, UT=8) and quiet (blue line, UT=4) conditions. A dipole magnetic field is also plotted (black line). The mirror points correspond to an equatorial pitch angle of $\alpha_{eq} = 30$ degree.

Table 1. Wave spectrum and plasma parameters at L=4.25, for various magnetic local times (MLTs).

|	ω_m/Ω_{ce}	$\delta\omega/\Omega_{ce}$	$|\lambda|$	$n_e(cm^{-3})$	$<B_w>(pT)$
04 MLT	0.25	0.1	$< 10°$	9.3	100
08 MLT	0.23	0.1	$< 15°$	9.5	100
12MTL	0.21	0.08	$< 45°$	13.5	100
16MTL	0.2	0.08	$< 45°$	17.4	100
20MLT	0.2	0.06	$< 25°$	17.2	100
24MLT	0.22	0.08	$< 10°$	13.1	100
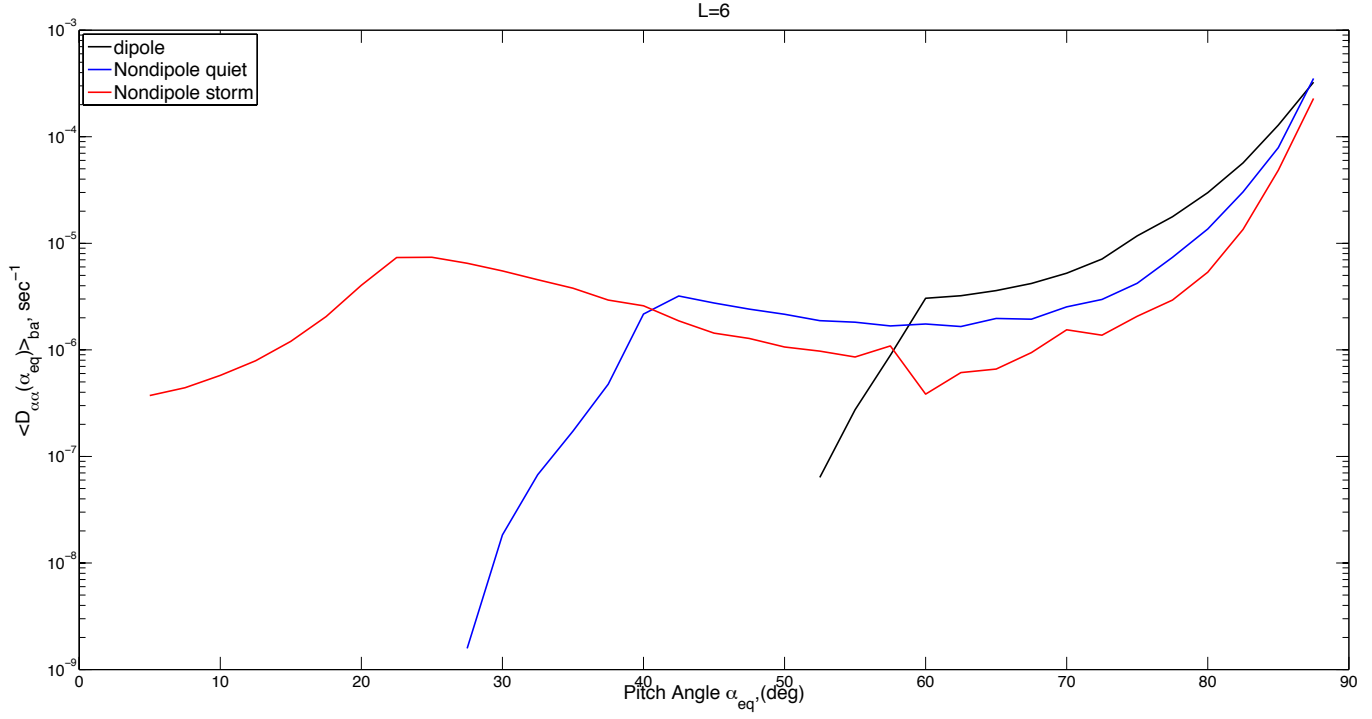
Figure 3.   Bounce-averaged pitch angle diffusion coefficients as a function of equatorial pitch

angle, computed at $L = 6$. The black line corresponds to the dipole field, the blue line is for

the magnetic field obtained from RAM-SCB for quiet conditions and the red line is for storm

conditions.
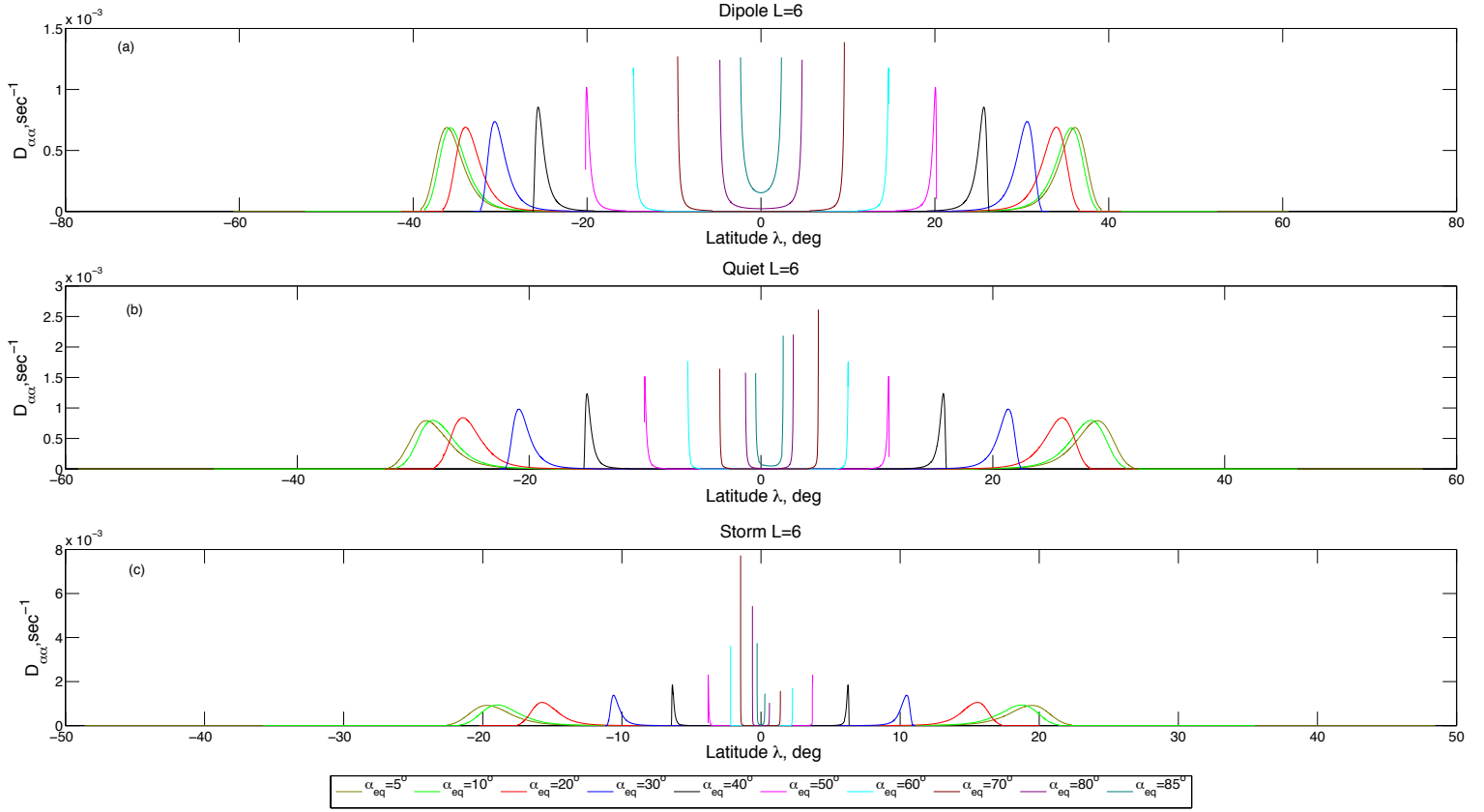
Figure 4. The local pitch angle diffusion coefficients versus magnetic latitude along the field line for different equatorial pitch angles and for the dipole magnetic field (a) and the RAM-SCB magnetic field for quiet (b) and storm (c) condtions.
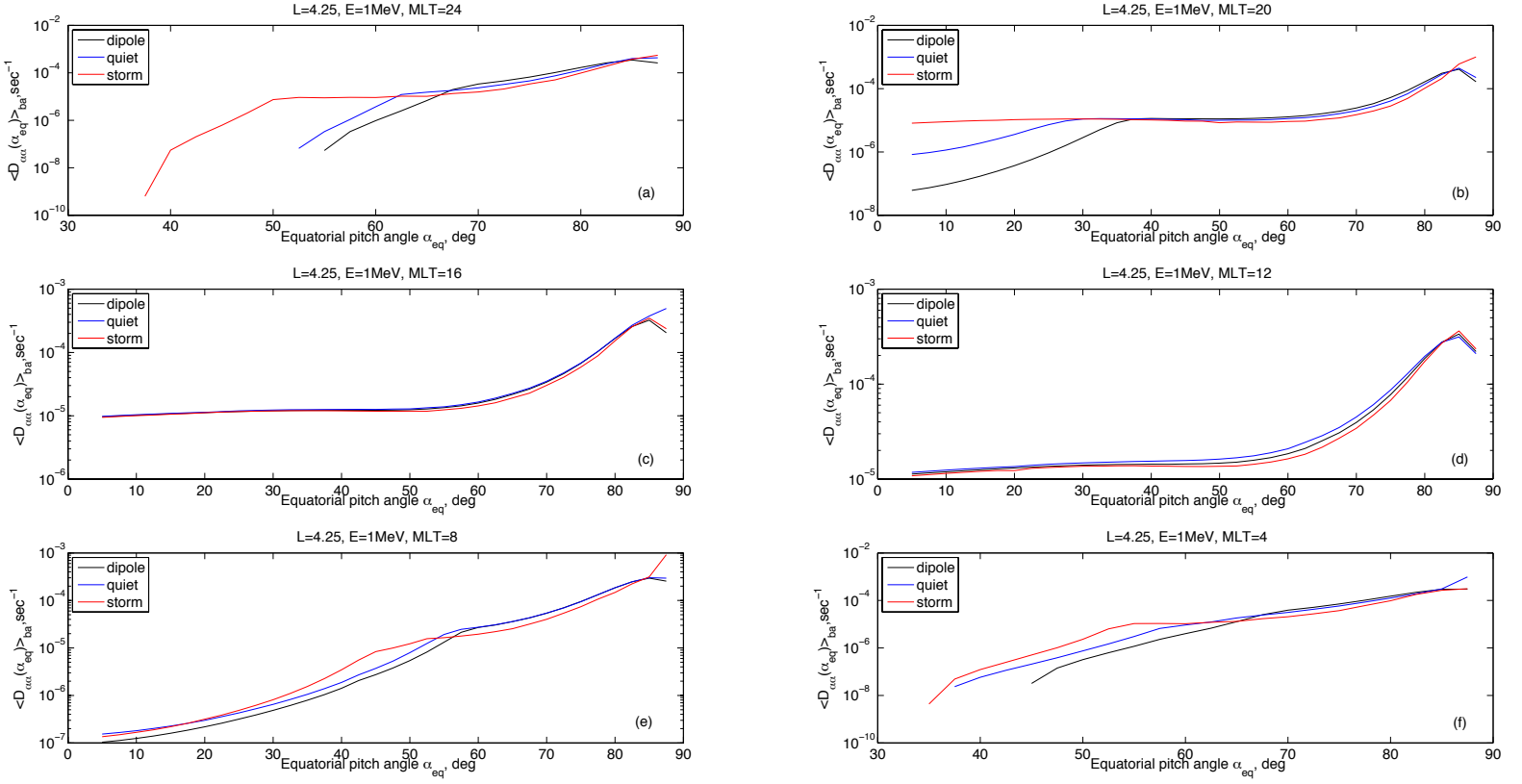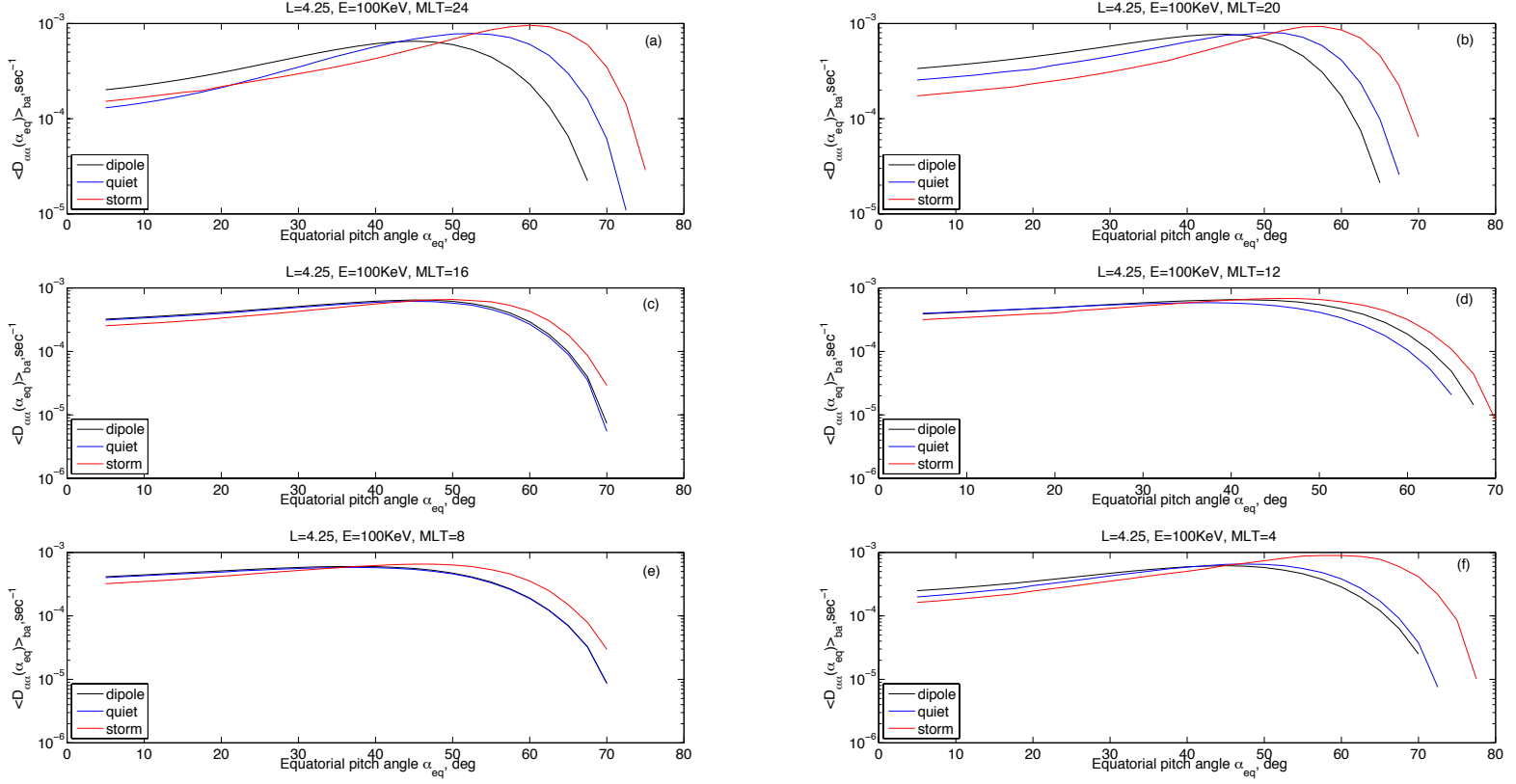
Figure 5.   Bounce-averaged pitch angle diffusion coefficients as a function of equatorial pitch angle, computed at $L = 4.25$ for electron energy E = 1 MeV. The black line is for the dipole magnetic field, the blue line is for the RAM-SCB magnetic field for quiet conditions and the red line is for the RAM-SCB magnetic field for storm conditions. Figures (a) to (f) correspond to MLT=24, 20, 16, 12, 08, 04, respectively.
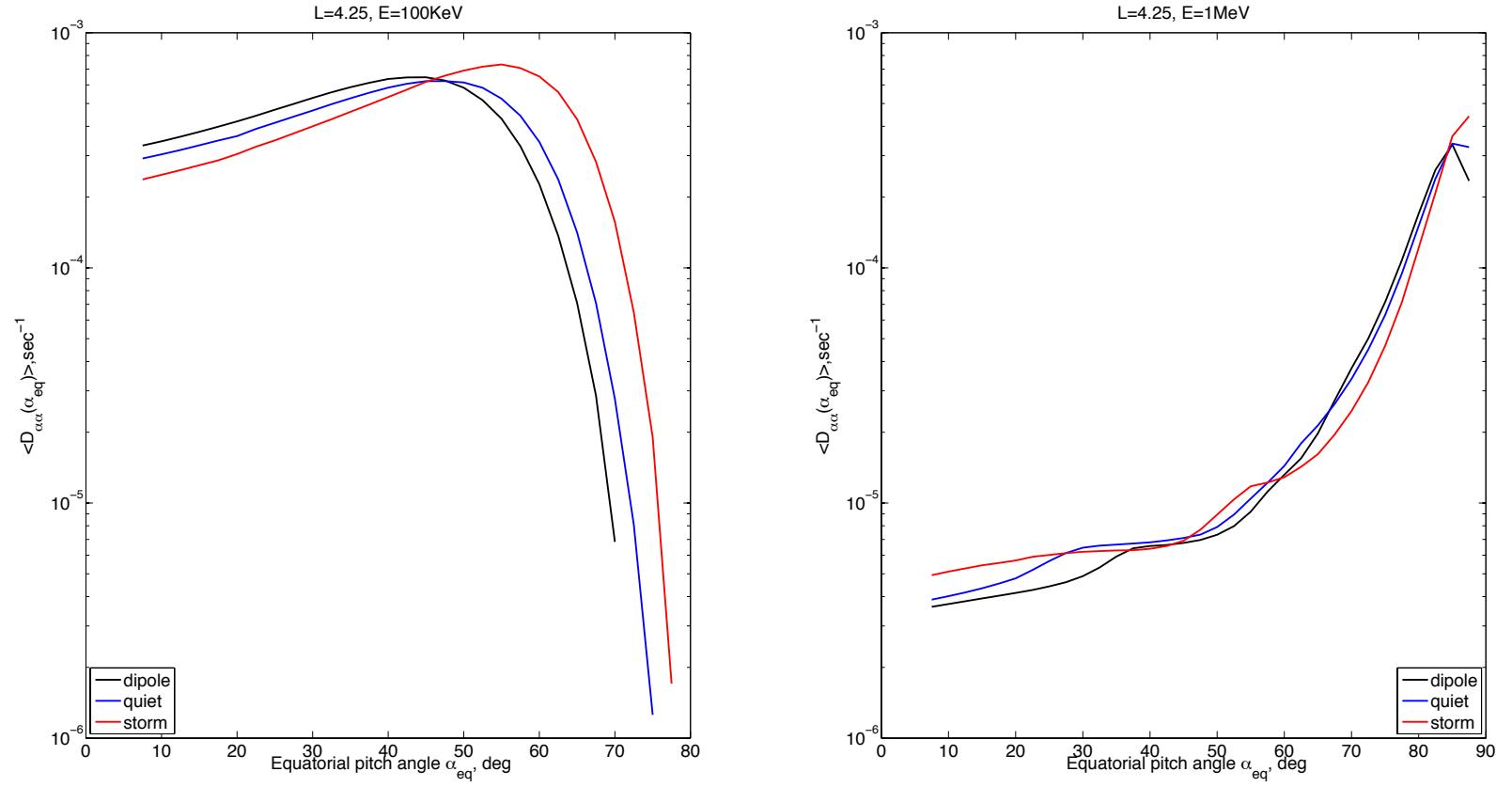
Figure 6. Bounce-averaged pitch angle diffusion coefficients as a function of equatorial pitch angle, computed at $L = 4.25$ for electron energy E = 100 keV. The black line is for the dipole magnetic field, the blue line is for the RAM-SCB magnetic field for quiet conditions and the red line is for the RAM-SCB magnetic field for storm conditions. Figures (a) to (f) correspond to MLT=24, 20, 16, 12, 08, 04, respectively.

Figure 7.   MLT-averaged pitch angle diffusion coefficients as a function of equatorial pitch angle: (a) corresponds to the electron energy E = 100 keV and (b) is for E = 1 MeV, respectively.
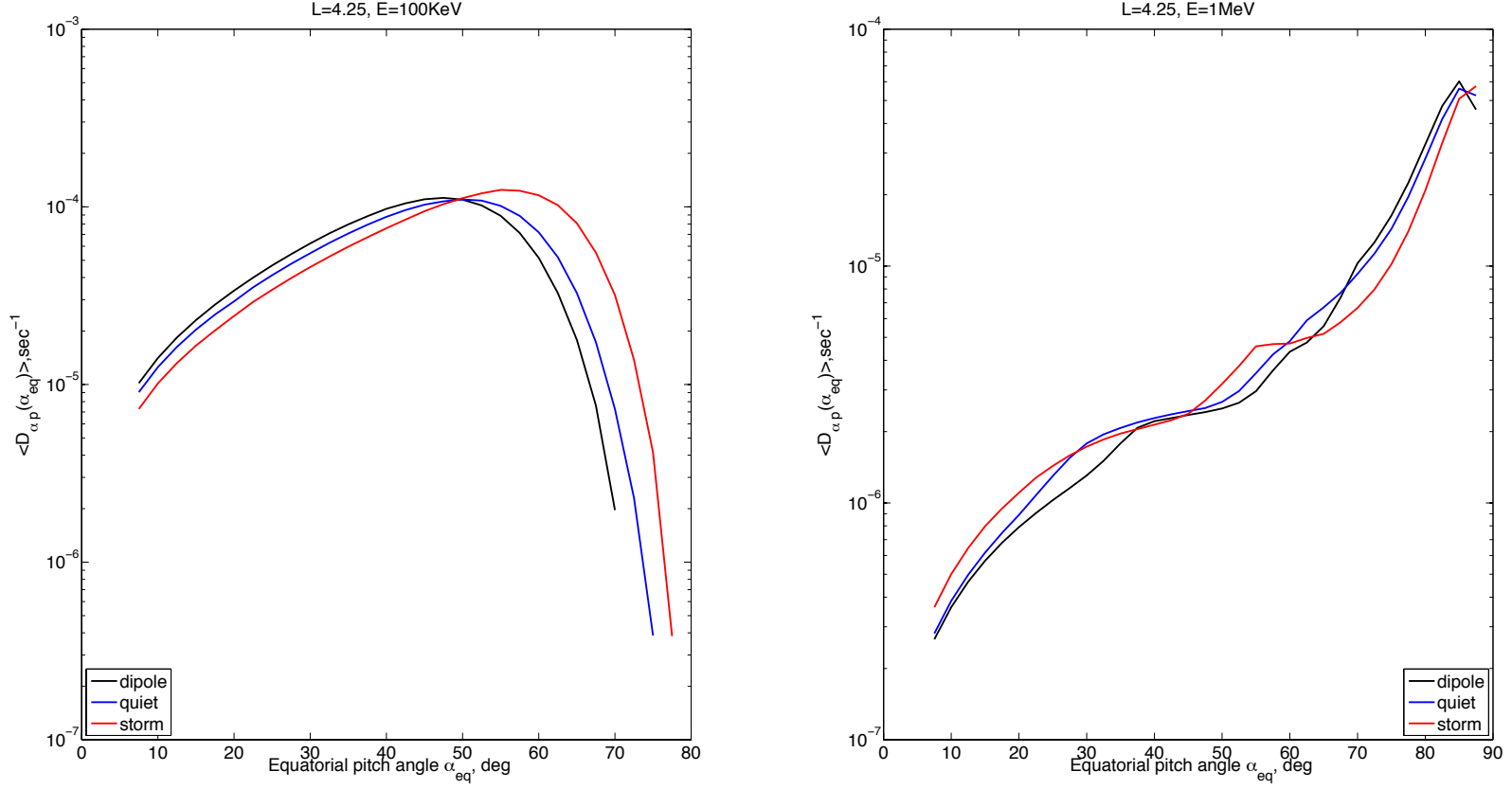
Figure 8. MLT-averaged mixed term diffusion coefficients as a function of equatorial pitch angle: (a) corresponds to the electron energy $E = 100$ keV and (b) is for $E = 1$ MeV, respectively.
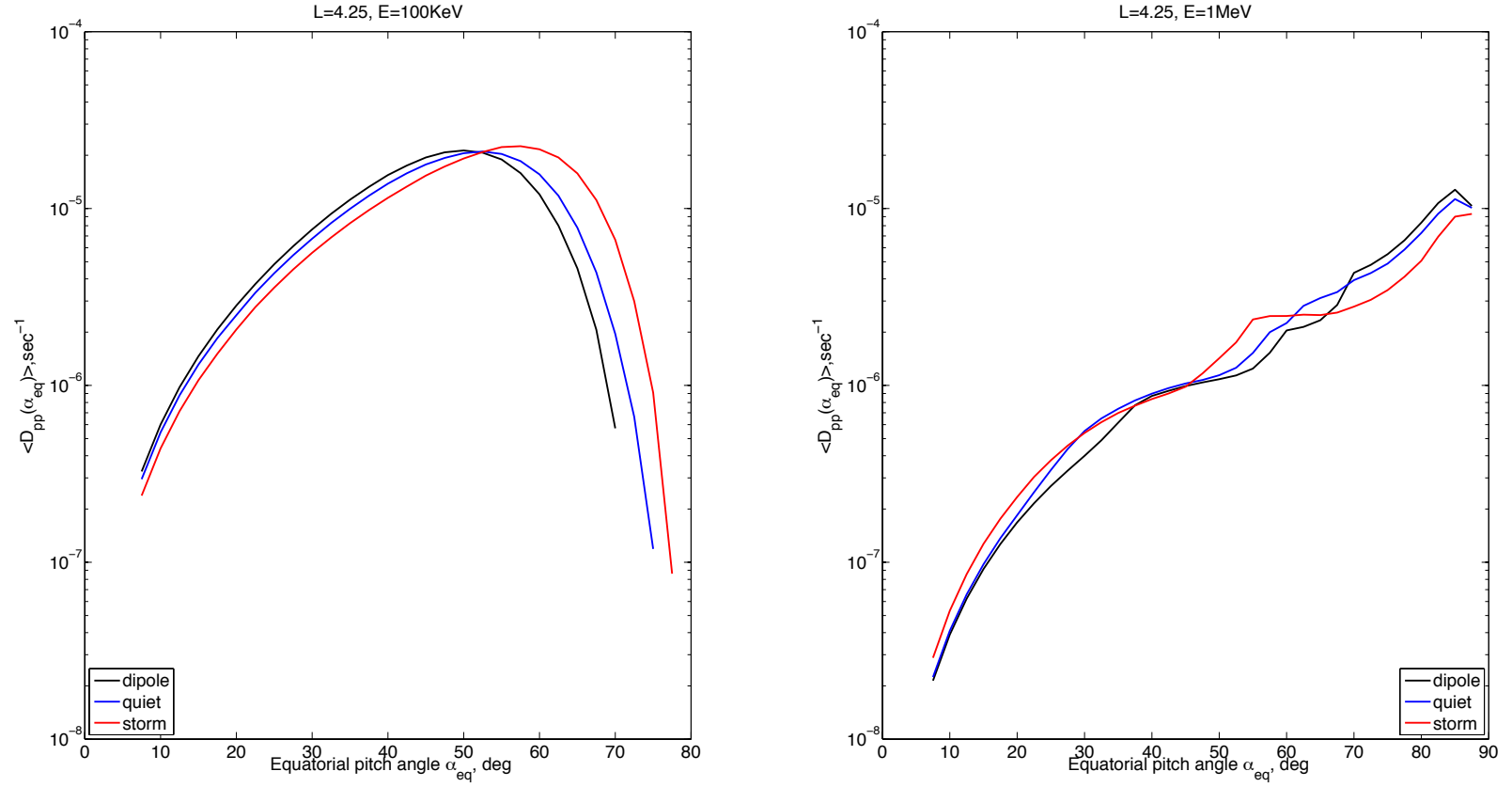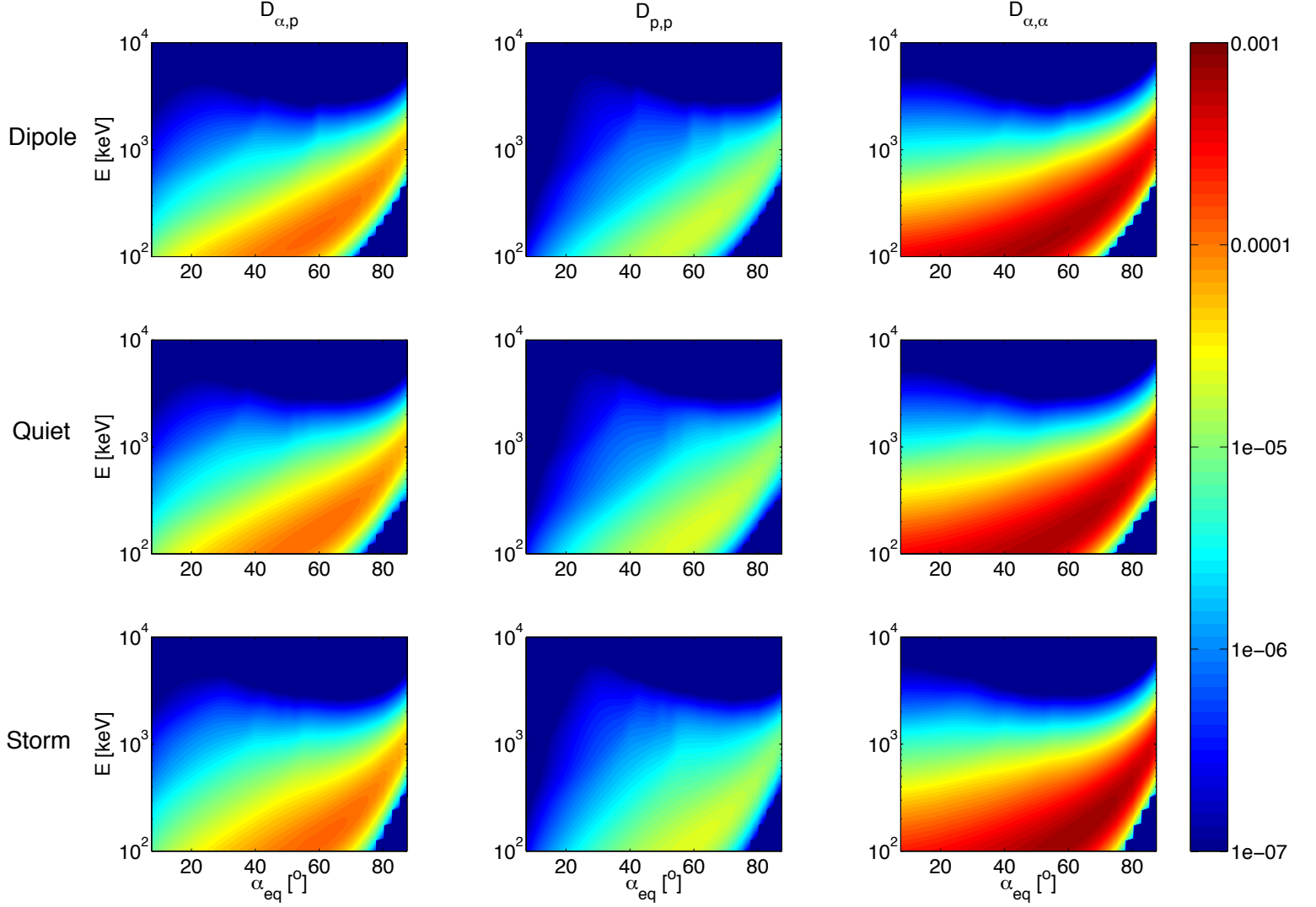
Figure 9.   MLT-averaged momentum diffusion coefficients as a function of equatorial pitch angle: (a) corresponds to the electron energy $E = 100$ keV and (b) is for $E = 1$ MeV, respectively.

Figure 10.   MLT-averaged pitch angle, energy and mixed term diffusion coefficients as a funtion of equatorial pitch angle (α_{eq}) and electron energy (E) at $L = 4.25$ for three magnetic field configurations: dipole magnetic field, RAM-SCB magnetic field for quiet and storm conditions.
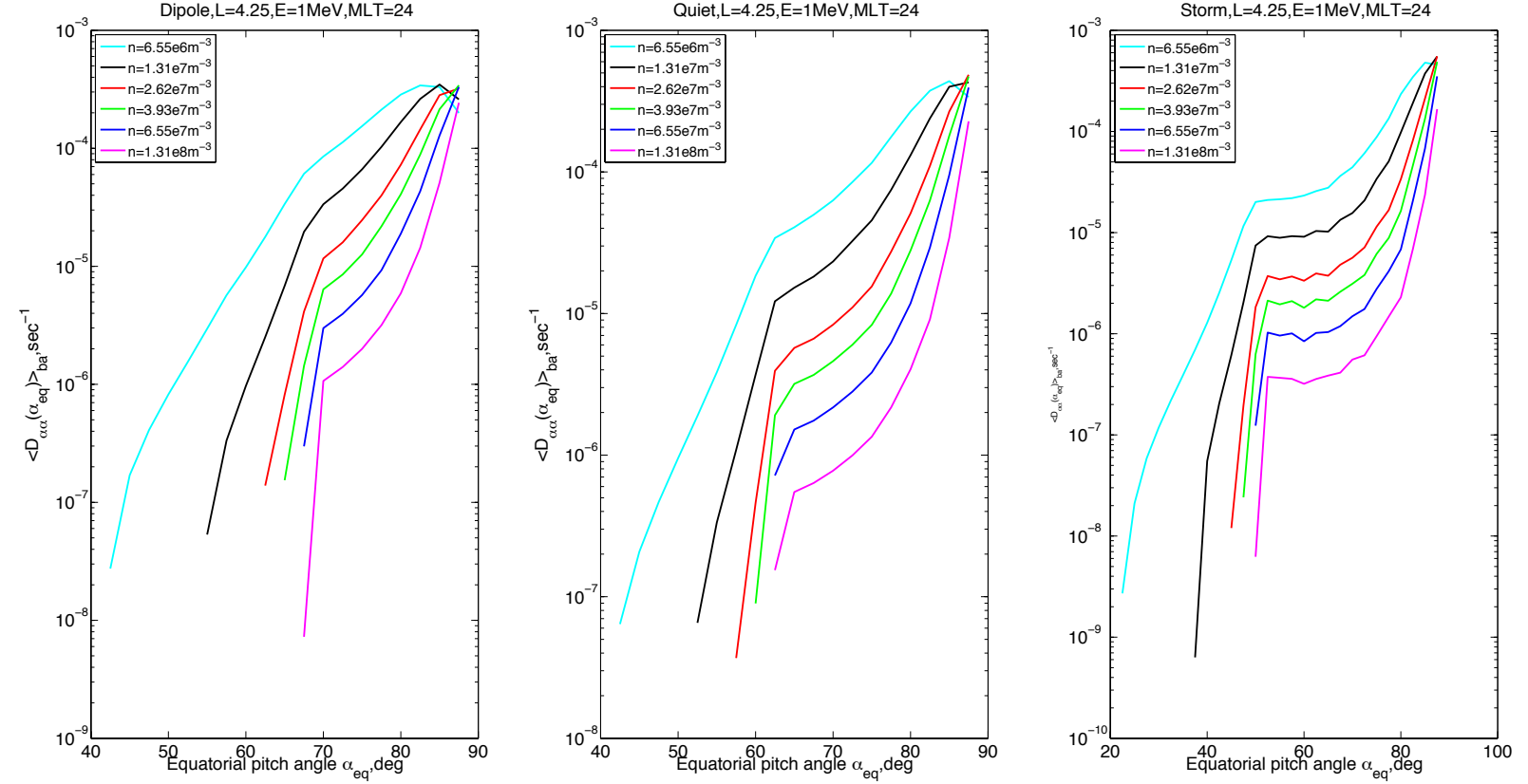
Figure 11.   Bounce-averaged pitch angle diffusion coefficients changes for different electron density and storm, quiet and dipole magnetic field configurations.